Heart

Computational Fractional Flow Reserve From Coronary Computed Tomographic Angiography: a new simplified model to predict severity of coronary artery lesions.

Journal:	*Heart*
Manuscript ID:	heartjnl-2014-306380
Article Type:	Original research article
Date Submitted by the Author:	18-Jun-2014
Complete List of Authors:	Tranter, David; University of Exeter, Engineering Clayton, Benjamin; Derriford Hospital, Radiology Tabor, Gavin; University of Exeter, Engineering Young, Philippe; University of Exeter, Engineering Shore, Angela; University of Exeter, Morgan-Hughes, Gareth; Derriford Hospital, Cardiology Iyengar, Srikanth; University of Plymouth, Peninsula College of Medicine & Dentistry Roobottom, Carl; Derriford Hospital, Radiology
Keywords:	ATHEROSCLEROSIS < CORONARY ARTERY DISEASE, FRACTIONAL FLOW RESERVE < CORONARY PHYSIOLOGY, CT SCANNING < IMAGING AND DIAGNOSTICS, CORONARY ANGIOGRAPHY < INTERVENTIONAL CARDIOLOGY

Computational Fractional Flow Reserve From Coronary Computed Tomographic Angiography: Comparison of diagnostic accuracy of a new simplified computational model to existing techniques.

Brief Title: A New Simplified Model for Computational CT FFR.

*David Tranter PhD
†Benjamin Clayton MD
*Gavin Tabor PhD
* Philippe G Young PhD
*Angela Shore PhD
†Gareth Morgan-Hughes MD
¶Srikanthe Iyengar MD
§‡Carl A Roobottom MD

*University of Exeter, Exeter UK.
†Department of Cardiology, Derriford Hospital, Plymouth UK.
¶ Department of Radiology, Wexham Park Hospital, UK
‡Department of Radiology, Derriford Hospital UK
§University of Plymouth Medical School, Plymouth UK.

This work was supported by an Open Innovation Platform – Proof of Concept Fund from the University of Exeter.

Phillippe G Young has a financial interest with Simpleware, the company that produce ScanIP used in data manipulation.

Corresponding Author
Professor Carl Roobottom.
Department of Imaging, Derriford Hopspital, Plymouth UK PL6 8DH
Tel. & Fax, 441752432517.
e-mail carl.roobottom@nhs.net

Keywords; computational fluid dynamics, coronary CT angiography, fractional flow re-serve, invasive coronary angiography

Word Count 3758 including abstract & references.

ABSTRACT

Aims: The aim of this feasibility study was to develop and investigate a new technique for measuring virtual fractional flow reserve (vFFR) based on computed tomographic coronary angiography (coronary CTA) imaging with simplistic fluid dynamic models.

Methods & Results: Two models of vFFR were developed, one simple (sFFR) and one more complex, designed to mimic existing vFFR models (tFFR). These models were tested on 28 lesions taken from the coronary CTA of 23 patients with known coronary artery disease who had also undergone ICA with measurement of invasive FFR. The sFFR and tFFR were then compared to the invasive FFR for the same lesions with ischemia defined as an invasive FFR < 0.80 .

Compared to invasive FFR the sensitivity, specificity, positive predictive value, negative predictive value and diagnostic accuracy of the simplified model were 0.84, 1.0, 1.0, 0.88, 0.93 respectively. The accuracy of sFFR was identical to tFFR.

Conclusions: We have developed a new computationally simpler method for obtaining a vFFR using new geometric and physics models that drastically reduces computational time. Applying a more complex physics model did not improve the diagnostic accuracy.

INTRODUCTION

Coronary computed tomographic angiography (coronary CTA) is a non-invasive test that allows direct visualization of coronary artery disease (CAD) and represents a viable alternative to invasive coronary angiography (ICA). Both modalities are limited to anatomical assessment, which correlates poorly with hemodynamic significance. [1-5].

Fractional flow reserve (FFR) is a dimensionless measurement, obtained during invasive angiography, which reflects the potential hemodynamic severity of stenoses [6]. It is defined as the ratio between the maximal blood flows achievable in a stenotic artery and the normal maximal blood flow in the same vessel. When combined with the anatomical assessment from invasive angiography, FFR-guided therapy improves event-free survival and reduces unnecessary revascularization, compared to ICA alone. [7-11].

There is growing interest in the possibility of predicting the FFR value of stenotic lesions from non-invasive imaging, through the application of Computational Fluid Dynamics (CFD) techniques. CFD is a numerical modelling technique that can be used to analyze the mechanical properties of fluids and is used to study flow velocities, pressure gradients and shear wall stresses in vessels. CFD is a complex process involving the generation of a 3-dimensional model from the medical image dataset; this is broken down into thousands of smaller volumes (known as discretization) and boundary conditions, limiting the area of interest, are applied to the extracted model.

These processes are computationally intense and each step has the potential to introduce error.

The use of CFD to generate virtual, FFR (vFFR) from coronary CTA data using computationally intense methods has been explored [12] [13]. The DISCOVER-FLOW [14] and the more recent DeFACTO trials and NXT trials [15] [16] reported that vFFR adds to the diagnostic performance of to coronary CTA for stenosis assessment in all patients. Their reconstructions evaluated both the entire proximal coronary artery tree and myocardial mass and were computationally demanding, taking approximately 6 hours per examination on specialised, off-site computers.

More recent work using CFD on models generated from invasive angiography supports the concept that FFR may be accurately estimated using just the geometry of the isolated arterial branch. This technique produced close correlation between the computational and invasive FFR measurements (r=0.84) [17]. The disadvantage of this technique is its invasive nature and the requirement for rotational angiographic equipment, but it does lend support to the concept of less computationally demanding vFFR derivation.

The objective of this study was to investigate the performance of a new, less-demanding workflow that generates a vFFR from non-invasive, CT datasets. The new workflow uses a simplified steady state CFD model (sFFR) on geometrical models of the full length of an isolated diseased artery. The geometries were created using a voxel-based technique where imaging pixels

are selected, by a suitable Hounsfield unit threshold range, as opposed to traditional computer aided design methods.

In this study we also applied CFD models similar to previous efforts based on transient lumped parameter models (tFFR) to the same geometries to compare diagnostic and statistical accuracy of the two techniques.

METHODS

Study design

This study was conducted at a single, high-volume, tertiary cardiothoracic centre (Derriford Hospital, Plymouth, United Kingdom) and recruited from a larger study examining the use of high-definition coronary CTA in the high-risk population from 2011-12. The regional Research Ethics Committee approved the study and all patients gave informed consent. Subsequent data processing and analysis was performed in a blinded fashion at the University of Exeter.

Study population

Patients undergoing invasive coronary angiography with a high pre-test probability of CAD were included. Exclusion criteria were patients under 40 years old, those requiring immediate percutaneous coronary intervention, elevated serum creatinine (>135 mmol/L) or estimated glomerular filtration rate <30ml/min/1.73m^2, contrast induced nephropathy, permanent or persistent atrial fibrillation, contraindication to intravenous beta-blockade, pregnancy or body mass index >33kg/m^2. Patients unable to hear or understand instructions in English were also excluded.

Patients who underwent ICA with invasive FFR for clinical reasons were included in this analysis.

Procedure protocol

Invasive coronary angiography was undertaken in accordance with standard clinical practice (Catheter lab - Philips Allura Xper FD-10, Philips Healthcare, Best, Netherlands). Each coronary artery was visualised in at least two orthogonal planes using standard projections, with additional views undertaken for overlapping segments or unusual anatomy. Stenosis assessment was facilitated with proprietary quantitative coronary analysis software (View Plus, Sanders Data Systems, California, USA).

FFR was performed at the time of ICA. Investigators performed FFR in vessels deemed clinically indicated. Hyperemia was induced by an intravenous infusion of adenosine at the rate of 140 μg/kg/min and arteries were interrogated with a standard pressure wire (PressureWire Aeris, Radi Medical Systems, Sweden).

All patients underwent high-definition, 64-slice coronary CTA (GE Healthcare, Discovery HD-750), within 28 days of ICA in a random order. Patients with a heart rate greater than 60 beats per minute received intravenous metoprolol, to achieve a heart rate of <60 beats per minute. Coronary CTA was performed using prospective ECG gating, 350ms gantry rotation time, 64 x 0.625mm slice collimation, 80-120 kV tube voltage, BMI-adapted fixed tube current (BMI < 22.5 kg/m^2: 450 mA, BMI 22.5 – 24.9 kg/m^2: 500mA, BMI 25.0 – 27.4 kg/m^2: 600 mA, BMI 27.5 - 30 kg/m^2: 700 mA, BMI >30 kg/m^2: 800 mA). A dual-phase contrast injection protocol was used with 100 ml of Ioversol (Optiray-350, Mallinckrodt Inc., Hazelwood, MO,

USA) at 6.5 ml/s followed by a 50ml saline flush using a standardised protocol.

Generating the geometric model

28 lesions from 23 DICOM datasets were imported into third party software (ScanIP, Simpleware, Exeter, UK) for processing. Methods based on threshold values of the pixels and connectivity algorithms were used to provide a surface model of the diseased artery using a voxel-based technique as opposed to traditional computer aided design based modelling. All models consisted of the isolated, full-length diseased artery with all bifurcations ignored. The position of the distal pressure sensor was obtained from the ICA images and used to establish which pressure to use in the simulated pressure fields. A typical workflow output to create the geometric model is shown in Figure 1.

Computing the sFFR

Two different CFD models were implemented as part of this study. In the first we applied a computationally simple steady state, Newtonian model with a constant velocity inlet and zero pressure outlet. This does not involve defining parameters that model the downstream behaviour. The model demands no assumptions of the hemodynamics of the patient and the pressure field is entirely defined by the geometry of the patient's vessel. The model needs the full length of the artery so that the full patient-specific resistance to flow is included. The finite volume method of discretisation of

the Navier Stokes equation were solved using OpenFOAM (OpenCFD, Bracknell, UK), a free, open source CFD software package. After convergence the vFFR was calculated from the simulation pressure fields. In the steady model the sFFR was calculated directly from the steady state pressures proximally and distally to the lesion.

Computing the tFFR

Secondly we applied the more complex modelling to the same data. This transient model was made up of a pulsatile velocity inlet and a 3 element Windkessel pressure outlet. The Windkessel model is a resistance-based model that relates pressure to resistance and flow rate. The model requires parameters that represent aortic characteristic impedance, peripheral impedance, and arterial compliance. These will be patient specific and need to be invasively obtained or estimated somehow. In this study these parameters were obtained from previous investigations that estimated values of resistance and compliance in the coronary network [18]. The finite volume method of discretisation of the Navier Stokes equation were again solved using Open-FOAM. After convergence the vFFR was calculated from the simulation pressure fields. In the transient model the tFFR was calculated from the temporal average of pressure proximally and distally to the lesion.

Statistical analysis

The primary study end point was the diagnostic accuracy of vFFR compared to invasive FFR as the reference standard. Sensitivity, specificity, positive predictive value, negative predictive value and the r squared value of the

correlation between vFFR and invasive FFR against a linear curve passing through the origin were calculated for both computational techniques. The 95% confidence intervals were calculated using the Agresti-Coull interval for smaller samples [19].

RESULTS

Patient characteristics.

The patients were part of a study looking at the use of CT in the high-risk population. Unsurprisingly therefore the population was predominantly male with a high-risk profile (see table 1). Of note was the high prevalence of coronary artery calcification. Only eight patients had an Agatson score of <400 and 6 had an Agatson score of >1000. All but two patients had a single vessel stenosis and two had double vessel disease. No patients in the group had sequential stenoses. Image quality of the CT was good in all examined segments.

Comparison of steady state FFR versus invasive FFR data.

The mean difference between sFFR and invasive FFR data was 0.02. Figure 2 shows the comparison between computationally derived FFR (both simple and transient) and the invasive FFR data. For steady simulations sensitivity, specificity, positive predictive value, negative predictive value (95% CI) and diagnostic accuracy compared to invasive FFR was as follows 0.84 (0.57,0.95), 1 (0.79, 1.0), 1 (0.74,1.0), 0.88 (0.65,0.96) and 0.93.

Figure 3 shows the correlation between sFFR values against the invasive FFR values. The r-value of the correlation between steady and experimental data against a linear curve passing through the origin was 0.73.

The typical computational time for the steady simulations was 10 minutes on a standard desktop PC.

Comparison of transient state FFR versus invasive FFR data.

The mean difference between transient and experimental data was 0.01. For tFFR simulations sensitivity, specificity, positive predictive value, negative predictive value (95% CI) and diagnostic accuracy compared to invasive FFR was as follows 0.84 (0.57,0.95), 1 (0.79, 1.0), 1 (0.74,1.0), 0.88 (0.65,0.96) and 0.93.

Figure 4 shows the correlation between tFFR values against invasive FFR values. The r-value of the correlation between transient and experimental data against a linear curve passing through the origin was 0.82. The typical computational time for the transient simulations was approximately 24 hours on the same computer.

Comparison of steady versus transient data

Figure 2 shows a bar graph of transient, steady and invasive results for each FFR case. Figure 5 shows a Bland Altman Plot between steady and transient results for each lesion.

DISCUSSION

We have developed a new workflow that allows the processing of CT data to construct highly accurate geometries of diseased coronary arteries for CFD analysis. This accurate geometry was achieved by two factors. Firstly we used voxel-based imaging techniques to generate a 3D geometric model. This method is based on threshold values of the pixels and connectivity algorithms to provide a surface model of the diseased artery as opposed to traditional computer aided design based modelling. In the voxel-based approach pixels lying in a grey scale range that corresponded to the vessel are grouped and then connectivity algorithms are applied to fully isolate the target pixels. Further computer graphics algorithms adjust these three dimensional volume elements using local interpolation. This final step notably increases the subvoxel accuracy of the model, especially in reducing the error because of the partial volume effect [20] [21]. This is in contrast to traditional computer aided design based modelling where edge detection algorithms attempt to capture the bounding surface of the geometry, a process that can be time consuming, not very robust and potentially impossible for complex topologies or for image data of limited quality [22].

Secondly, in contrast to other studies using CT data we made efforts to reconstruct the whole of the isolated artery rather than only the proximal segment. By modelling the entire length of the arterial branch we are using the full patient specific contributions to resistance to the flow. The more

proximal the outlet boundary conditions are set, the more computational modelling required of the distal conditions. This not only increases computational time but also requires more assumptions about distal boundary conditions that are a potential source of error.

Once the model was created CFD simulations by OpenFOAM allowed us to apply either steady state (where pressure gradients are constant) or transient models (using complex pressure modelling). The resultant pressure fields were then used to generate a virtual FFR for both scenarios. The rationale for this was to see if the more complex modelling techniques conferred any advantage.

Both models produced results that agreed equally well with the procedural data. In particular, the transient CFD model did not improve diagnostic accuracy compared with the steady state model. The transient model gave identical diagnostic accuracy and statistical indicators. The standard deviation from the two models is 0.02 with the mean difference being 0.007. In contrast however computational time is very different. The steady state model takes only 10 minutes, a fraction of the computational time of the transient model (24 hours) on the same computer.

Advantages of simple algorithm.

FFR values generated by our steady state simulation are an alternative, non-invasive method that can be used to generate vFFR data. As with other computational techniques there is no need to subject the patient to

hyperaemia and, as with other techniques that use CT data the technique is non-invasive. In contrast however our steady state model is computationally simple and uses widely available software to generate vFFR. All the software used in our study is readily available, either commercially or as open source software. This allows the development of tools that can run on standard PC hardware, which could be made accessible to clinicians with results that could be available at the same attendance as the CT scan. Its simplicity offers the option of incorporating vFFR onto CT workstations and PACS systems so vFFR can be estimated at the time of image analysis.

Limitations of technique.

Since this reconstruction method is dependent on generating highly accurate geometries from medical images of the whole vessel the quality of the images is critical. This is a factor that has been recognised by other workers [16]. Poor contrast, low resolution images or images that contain artefacts represent a significant challenge in constructing accurate geometries. In addition this preliminary study only considered a small number of cases with a single stenosis in each vessel. It is possible that more complex simulations are superior in cases with multiple stenotic segments. It is also possible that in cases with abnormal myocardium (say vessels supplying areas of myocardial infarction) may introduce error. However the agreement obtained with the simplified model suggest that further investigation into this method of generating vFFR is warranted.

Acknowledgements

This work was supported by an Open Innovation Platform – Proof of Concept Fund from the University of Exeter.

Conflicts of Interest

Philippe Young is a Director at Simpleware, and has a financial interest in Simpleware Ltd, the company that develops and markets the image processing software package ScanIP used in the segmentation and model construction.

The other authors have no conflict of interest.

References

1. Chow, BJW, Abraham A, Wells AG et al. Diagnostic accuracy and impact of Computed Tomographic coronary angiography on utilization of invasive coronary angiography. Circulation: Cardiovascular Imaging 2009; **2**: 16-23.

2. Min JK, Leslee J. Shaw and Daniel S. Berman. The present state of coronary computed tomography angiography: a process in evolution. J Am Coll Cardiology 2010; **55**: 957-965.

3. Meijboom BW, Van Mieghem CAG, van Pelt N Weustink A, Pugeliese F, Mollet NR, Boersma E, Regar E, van Gues RJ, Jaegere PJ, Serruys PW, Krestin GP, deFeyter PJ. Comprehensive assessment of coronary artery stenosis computed tomography coronary angiography versus conventional coronary angiography and correlation with fractional flow reserve in patients with stable angina. J Am Coll Cardiol. 2008;**52**,:636-643.

4. Miller JM, Rochitte CE, Dewey M, Arbab-Zadeh A, Niinuma H, Gottlieb I, Paul N, Clouse ME, Shapiro EP, Hoe J, Lardo AC, Bush DE, de Roos A, Cox C, Brinker J ,Lima JAC. Diagnostic performance of coronary angiography by 64-row CT. New Eng J Med 2008; **359**: 2324-2336

5. Budoff MJ, Dowe D, Jollis JG Gitter M, Sutherland J, Halamert E, Schere M, Bellinger R, Martin A, Benton R, Delago A Min JK. Diagnostic performance of 64-multi detector row coronary computed tomographic angiography for evaluation of coronary artery stenosis in individuals without known coronary artery disease results from the prospective multicenter ACCURACY (assessment by coronary computed tomographic angiography of individuals

undergoing invasive coronary angiography) trial 2008. J American Coll Cardiol**. 52**,:1724-1732.

6. Pijls Nico hj, van Son JA, Kirkeeide RL, DeBrruyne B, Gould KL. Measurement of fractional flow reserve to assess the functional severity of coronary-artery stenoses. New Eng J Med 1996; **334**,:1703-708.

7. Tonino PA, DeBruyne B, Pijls NH, Siebert U, Ikeno F. vant Meer M, Klauss V, manhonoran G, Engstrom T, Oldroyd KG, Van Leer PN, MacCarthy PA, Fearon WF. Fractional flow reserve versus angiography for guiding percutaneous coronary intervention. New Eng J Med 2009; **360**: 213-24.

8. Tonino PA Fearon WF, De Bruyne B, Oldroyd KG, Leesar MA, Ver Lee PN, MacCarthy PA, vant Veer M, Pijls NHJ. Angiographic versus functional severity of coronary artery stenoses in the FAME Study fractional flow reserve versus angiography in multivessel evaluation. J Am Coll Cardiol. 2010; **55**: 2816-2821.

9. De Bruyne B, Baudhuin T, Melin JA, Pijls NH, Sys SU, Bol A, Paulus WJ, Hendrickxs GR, Wijns W. Coronary flow reserve calculated from pressure measurements in humans. Validation with positron emission tomography. Circulation 1994; **89**: 1013-1022.

10. Berger A, Botman K-J, MacCarthy PA, Wijns W, Bartunek J, Hendrickx GR, Pijls NHJ, De Bruyne B. Long-term clinical outcome after fractional flow reserve-guided percutaneous coronary intervention in patients with multi vessel disease. J Am Coll Cardiology 2005; **46**: 438-442.

11. Pijls NH, van Son JA, Kirkeeide RL, De Bruyne B Gould KL. Experimental basis of determining maximum coronary, myocardial, and collateral blood flow by pressure measurements for assessing functional stenosis severity

before and after percutaneous transluminal coronary angioplasty. Circulation 1993; **87**: 1354-367.

12. Zarins CK, Taylor CA and Min JK. Computed fractional flow reserve (ffct) derived from coronary ct angiography. J Cardiovas Trans Research 2013; 1-7.

13. Kim HJ, Jansen KE, and Taylor CA. Incorporating auto regulatory mechanisms of the cardiovascular system in three-dimensional finite element models of arterial blood flow. Annals of Biomedical Engineering 2010; **38**: 2314-2330.

14. Koo Bon-Kwon, Erglis A, Joon-Hyung D Daniels DV, Jagere S, Hyo-soo Kim, Dunning A, DeFrance D, Lansky A, Leipsic J, Min JK. Diagnosis of ischemia-causing coronary stenoses by noninvasive fractional flow reserve computed from coronary computed tomographic angiograms results from the prospective multicenter discover-flow (diagnosis of ischemia-causing stenoses obtained via noninvasive fractional flow reserve) study. J Am Coll Cardiol. 2011;**58**,:1989-1997

15. Min JK, Leipsic J, Pencina MJ Berman DS, Koo B_W, van Mieghem C, Erglis A, Lin FY, Dunning AM, Apruzzese P, Buddoff MJ, Cole JH, Jaffer FA, Leon MB, Malpeso J, Mancini GBJ, Park S-J, Schwartz RS, Shaw LJ, Mauri L . Diagnostic accuracy of fractional flow reserve from anatomic CT angiography fractional flow reserve from CT angiography. JAMA 2012; **308**: 1237-1245.

16. Nørgaard BL, Leipsic J, Gaur S, Seneviratne S, Ko BS, Ito H, Jensen JM,Mauri L, De Bruyne B, Bezerra H, Osawa K, Marwan M, Naber C, Erglis A, Park S-J, Christiansen EH, Kaltoft A, Lassen JF, Bøtker HE, Achenbach S. Diagnostic performance of non-invasive fractional flow reserve derived from coronary CT angiography in suspected coronary artery disease: The NXT trial, J

Am Coll Cardiol (2014), doi: 10.1016/j.jacc.2013.11.043.

17. Morris P,Ryan D, Morton AC, Lycett R, Lawford PV, Hose R, Gunn JP . Virtual fractional flow reserve from coronary angiography: Modeling the significance of coronary lesions. Results from the virtu-1 (virtual fractional flow reserve from coronary angiography study).
J Am Coll Cardiol.: Cardiovascular Interventions 2012; **6**: 149-157.

18. Kim H.J, Vignon-Clementel E, Coogan JS, Figueroa CA, Jansen KE & Taylor CA. Patient-specific modelling of blood flow and pressure in human coronary arteries. Annals of Biomedical Engineering 2010; **38**: 3195-3209.

19. Agresti A and Coull BA. Approximate is better than exact for interval estimation of binomial proportions. The American Statistician 1998; **52:** 119-126.

20 Lorensen, William E., and Harvey E. Cline. "Marching cubes: A high resolution 3D surface construction algorithm." Computer Graphics 1987; **21**: 163-9

21 Cebral, JR, and Löhner R. "From medical images to anatomically accurate finite element grids." International Journal for Numerical Methods in Engineering 2001; **51.8** : 985-1008.

22. Young, PG, Beresford-West TBH, Coward SRL, Notarberardino B, Walker B, Abdul-Aziz A. "An efficient approach to converting three-dimensional image data into highly accurate computational models." Philosophical Transactions of the Royal Society A: Mathematical, Physical and Engineering Sciences 2008; **366**:3155-3173.

Legends for figures

Figure 1: Example of geometry construction for a LAD

Caption: Original CT data is imported (B) and segmentation based on threshold values of the pixels and connectivity algorithms gives a subset of pixels that represent the target vessel (C). These pixels then represent voxels in three-dimensional space whereby further algorithms employ local interpolation to create a high fidelity model (D). Comparison with the angiogram image (A) allows for confirmation of geometry and for knowledge of the pressure wire location. Following this the CFD model is produced from which pressure measurements are taken.

Figure 2: Computational models compared with invasive data. Procedural results (blue) compared with steady state (orange) and transient (yellow)

Figure 3

Correlation between Steady state model and invasive data with a linear curve of gradient 1 passing through the origin.

Figure 4

Correlation Between transient model and invasive data with a linear curve of gradient 1 passing through the origin.

Figure 5

Bland Altman Plot Difference between steady state data and transient data plotted against the mean value. The two horizontal lines represent two standard deviations away from the mean difference

Table 1. Baseline characteristic of patients (*Data are expressed as number (%) except where stated otherwise*)

	All included patients (N=23)
Age in years, mean (Range)	62(37-78)
Male gender	91 (75%)
Body mass index, mean (Range)	27 (17-33)
Hypertension	20(87%)
Diabetes	1 (4%)
Hypercholesterolemia	22(96%)
Smoking history	13 (57%)
Family history of CAD	6 (26%)
NYHA Status Class I Class II	 17 (74%) 6 (26%)
Calcium score (Agastson Units) Mean (Range)	810 (20-3140)

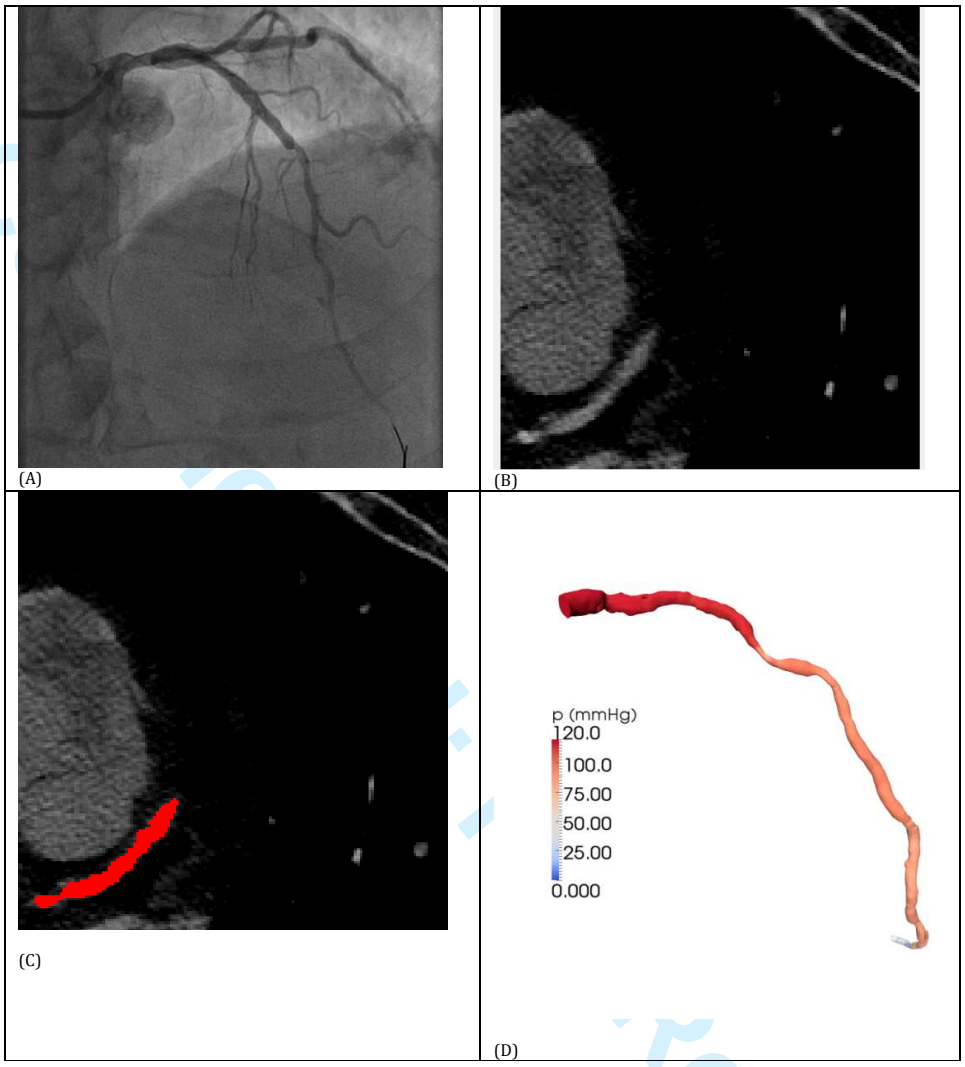

Figure 1 Title: Example of geometry construction for a LAD

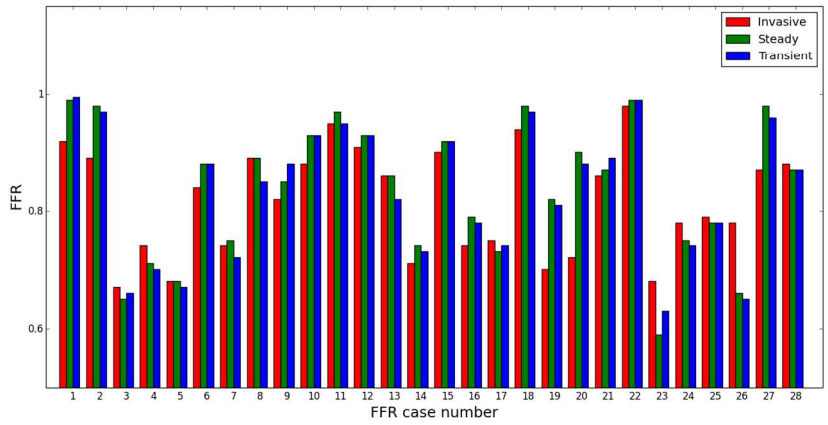

Figure 2: Computational models compared with invasive data.
Procedural results (blue) compared with steady state (orange) and transient (yellow)

433x206mm (100 x 100 DPI)

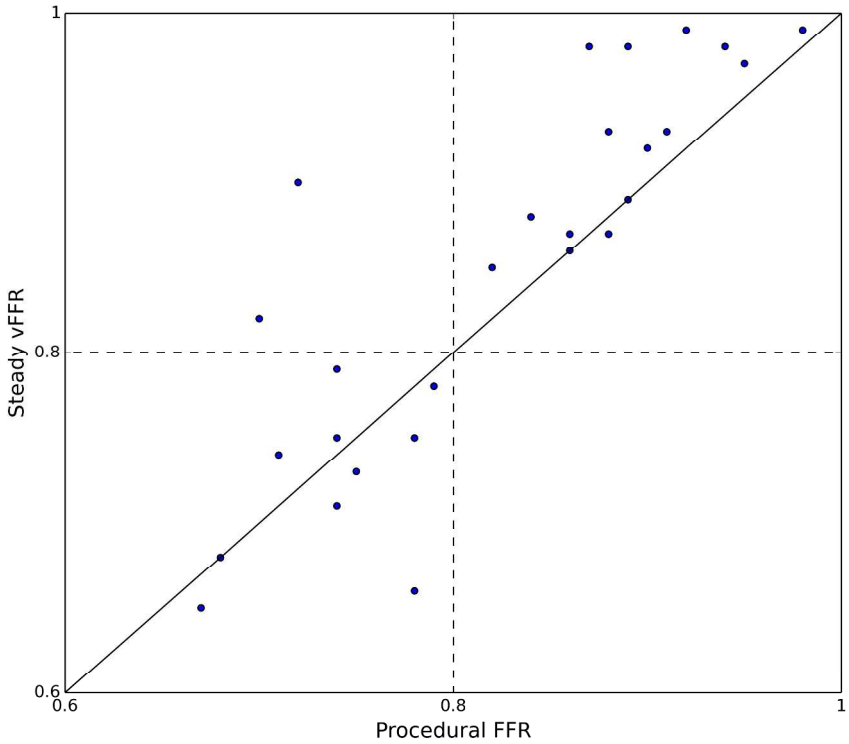

Figure 3
Correlation between Steady state model and invasive data with a linear curve of gradient 1 passing through the origin.

254x216mm (300 x 300 DPI)

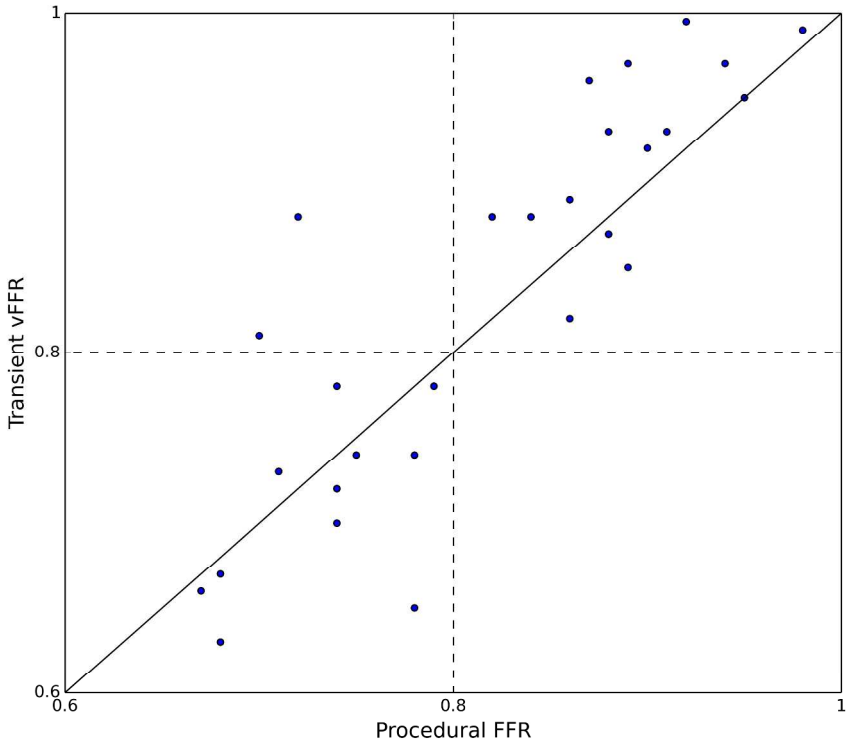

Figure 4
Correlation Between transient model and invasive data with a linear curve of gradient 1 passing through the origin.

254x216mm (300 x 300 DPI)

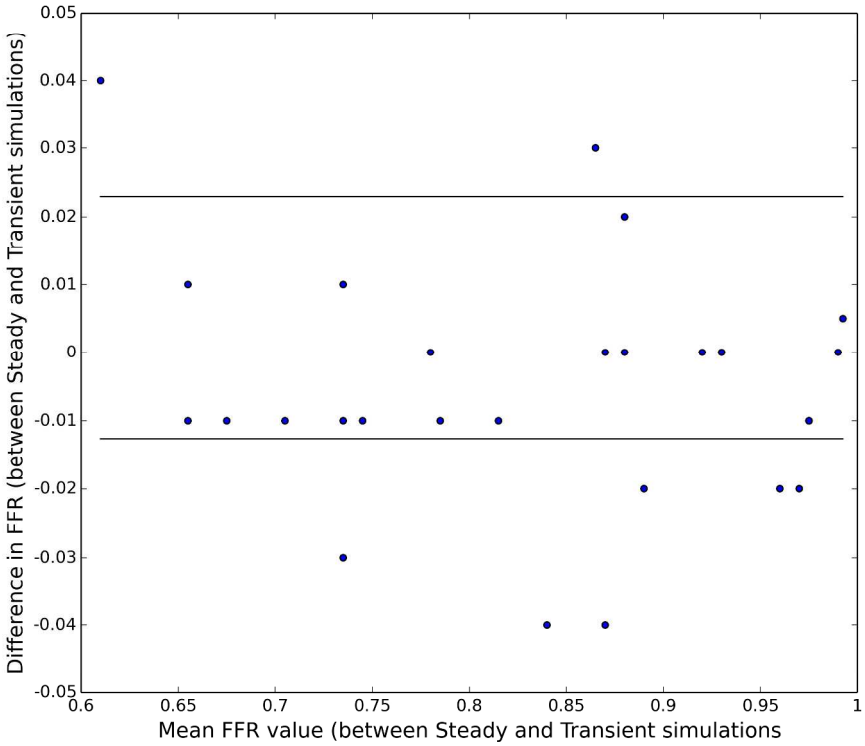

Figure 5
Bland Altman Plot Difference between steady state data and transient data plotted against the mean value. The two horizontal lines represent two standard deviations away from the mean difference

254x216mm (300 x 300 DPI)

STROBE Statement—checklist of items that should be included in reports of observational studies

	Item No	Recommendation
Title and abstract	1	(*a*) Indicate the study's design with a commonly used term in the title or the abstract-Feasibility study; see aims in abstract
		(*b*) Provide in the abstract an informative and balanced summary of what was done and what was found-done
Introduction		
Background/rationale	2	Explain the scientific background and rationale for the investigation being reported-paragraphs 1-3
Objectives	3	State specific objectives, including any prespecified hypotheses-paragraph 5 & 6
Methods		
Study design	4	Present key elements of study design early in the paper-done
Setting	5	Describe the setting, locations, and relevant dates, including periods of recruitment, exposure, follow-up, and data collection-done
Participants	6	(*a*) *Cohort study*—Give the eligibility criteria, and the sources and methods of selection of participants. Describe methods of follow-up *Case-control study*—Give the eligibility criteria, and the sources and methods of case ascertainment and control selection. Give the rationale for the choice of cases and controls *Cross-sectional study*—Give the eligibility criteria, and the sources and methods of selection of participants-done
		(*b*) *Cohort study*—For matched studies, give matching criteria and number of exposed and unexposed *Case-control study*—For matched studies, give matching criteria and the number of controls per case
Variables	7	Clearly define all outcomes, exposures, predictors, potential confounders, and effect modifiers. Give diagnostic criteria, if applicable-done
Data sources/ measurement	8*	For each variable of interest, give sources of data and details of methods of assessment (measurement). Describe comparability of assessment methods if there is more than one group-done
Bias	9	Describe any efforts to address potential sources of bias-done
Study size	10	Explain how the study size was arrived at-feasibility study
Quantitative variables	11	Explain how quantitative variables were handled in the analyses. If applicable, describe which groupings were chosen and why-done
Statistical methods	12	(*a*) Describe all statistical methods, including those used to control for confounding
		(*b*) Describe any methods used to examine subgroups and interactions
		(*c*) Explain how missing data were addressed-NA
		(*d*) *Cohort study*—If applicable, explain how loss to follow-up was addressed *Case-control study*—If applicable, explain how matching of cases and controls was addressed *Cross-sectional study*—If applicable, describe analytical methods taking account of sampling strategy
		(*e*) Describe any sensitivity analyses

Continued on next page

Results		
Participants	13*	(a) Report numbers of individuals at each stage of study—eg numbers potentially eligible, examined for eligibility, confirmed eligible, included in the study, completing follow-up, and analysed
		(b) Give reasons for non-participation at each stage
		(c) Consider use of a flow diagram
Descriptive data	14*	(a) Give characteristics of study participants (eg demographic, clinical, social) and information on exposures and potential confounders
		(b) Indicate number of participants with missing data for each variable of interest
		(c) *Cohort study*—Summarise follow-up time (eg, average and total amount)-done
Outcome data	15*	*Cohort study*—Report numbers of outcome events or summary measures over time
		Case-control study—Report numbers in each exposure category, or summary measures of exposure
		Cross-sectional study—Report numbers of outcome events or summary measures done
Main results	16	(*a*) Give unadjusted estimates and, if applicable, confounder-adjusted estimates and their precision (eg, 95% confidence interval). Make clear which confounders were adjusted for and why they were included-done
		(*b*) Report category boundaries when continuous variables were categorized
		(*c*) If relevant, consider translating estimates of relative risk into absolute risk for a meaningful time period NA
Other analyses	17	Report other analyses done—eg analyses of subgroups and interactions, and sensitivity analyses NA
Discussion		
Key results	18	Summarise key results with reference to study objectives-done
Limitations	19	Discuss limitations of the study, taking into account sources of potential bias or imprecision. Discuss both direction and magnitude of any potential bias-done
Interpretation	20	Give a cautious overall interpretation of results considering objectives, limitations, multiplicity of analyses, results from similar studies, and other relevant evidence
Generalisability	21	Discuss the generalisability (external validity) of the study results-done
Other information		
Funding	22	Give the source of funding and the role of the funders for the present study and, if applicable, for the original study on which the present article is based-done

*Give information separately for cases and controls in case-control studies and, if applicable, for exposed and unexposed groups in cohort and cross-sectional studies.

Note: An Explanation and Elaboration article discusses each checklist item and gives methodological background and published examples of transparent reporting. The STROBE checklist is best used in conjunction with this article (freely available on the Web sites of PLoS Medicine at http://www.plosmedicine.org/, Annals of Internal Medicine at http://www.annals.org/, and Epidemiology at http://www.epidem.com/). Information on the STROBE Initiative is available at www.strobe-statement.org.